A Numerical Analysis of Atmospheric Drag and Earth's J2 Perturbations in Near Earth Orbits

Dante Sanaei

Purdue University School of Aeronautics and Astronautics, West Lafayette, Indiana, 47906, USA

The following report develops a dynamic model for an artificial satellite under the perturbative effects of Earth's J2 parameter and atmospheric drag. This model is then numerically solved to propagate satellites in orbits that most require the inclusion of both perturbations: Sun Synchronous and Critically Inclined low-earth orbits. Orbital elements over long timespans are examined and drag induced orbital decay is studied to determine approximate lifetimes.

I. Introduction

The following analysis outlines the development and study of a dynamic model that incorporates perturbative accelerations from atmospheric drag and Earth's oblate shape to numerically propagate artificial satellites. Sun Synchronous and Critically Inclined orbits under 600 kilometers were chosen for analysis due to their necessity of Earth's J2 perturbation and their adverse susceptibility to atmospheric drag. From the numerical model, drift in orbital elements over long timespans and drag induced orbit decay were also examined.

Beginning from the Lagrange's Planetary Equations, a more practical set of relations were derived – termed Gauss's Variational Equations. These differential expressions of motion allowed for the inclusion of perturbative accelerations in the RSW coordinate system to the model. Importantly, the variables of interest generated from Gauss's equations are the Keplerian elements of the Earth orbiting object; thus, presenting the perturbative effects to size, shape, and orientation of the orbit in a more gradual and comprehensive manner. Force components from atmospheric drag and Earth's J2 effect are derived and inputted into Gauss's equations to form a final dynamic model.

Through numerical integration in MATLAB, initial orbital elements can be propagated forwards in time, and the effects of drag and Earth's oblate shape can be observed clearly.

The orbits that were chosen for examination held initial conditions that were formulated to optimize the effects of Earth's J2 perturbations on their trajectories. The two most popular of these are the Sun-Synchronous Orbit and the Critically Inclined Orbit. Both take advantage of perturbations from Earth's oblate shape to determine their initial inclination, therefore it is critical that the J2 effect be included in any model used in their study. Satellites in Sun-Synchronous Orbits are placed at an initial inclination that allows for the drift in the mean nodal precession to match Earth's rotation rate around the Sun; thus, allowing the orbit to maintain a constant solar orientation. A critically inclined orbit is one in which a satellite is placed at an initial inclination that will remove any drift of the mean argument of perigee – with the great benefit of reducing station keeping requirements.

In addition to Earth's oblate shape, low earth orbits are abundantly affected by atmospheric drag, and for this reason its effects are included in our model. With the assistance of a simplified standard atmosphere, the numerical integration models the gradual decay of the orbits – allowing for a general determination of a lifetime of the satellite. Analysis of drag induced decay and time until re-entry for the chosen orbits is also included.

Objects in low earth orbit experience the largest perturbative effects from drag and Earth's J2 parameter, therefore a dynamic model to accurately propagate and examine orbits of near-earth artificial satellites must include both at a minimum.

II. Background and Analysis

The following section will derive the dynamic model that is used to numerically propagate low earth orbit satellites in the presence of J2 and drag perturbations. In addition, derivation of critical and sun synchronous inclination will be discussed.

The derivations in Part A and B have been adapted from Longuski's AAE690 course notes [1]

A. Gauss's Variational Equations

We will begin by producing six differential equations that describe the behavior of a body's orbital elements in relation to time when under a perturbing force – these are referred to as Lagrange's Planetary Equations.

These equations can be derived from the following relation between Lagrange brackets of all six orbital elements and a disturbing function (R).

$$\sum_{k=1}^{6}[c_j, c_k]\dot{c_k} = \frac{\partial \mathrm{R}}{\partial c_j}, \qquad j = 1, \dots, 6$$

Where c_j and c_k are the Keplerian elements of a body. Given as: a (semimajor axis), e (eccentricity), i (inclination), ω (argument of periapsis), Ω (right ascension of ascending node), and a final fast changing element (we will use mean anomaly M).

The Lagrange brackets in the previous expression ($[c_j, c_k]$), can be solved to produce 15 relations between the elements and the disturbing function partials. Nine of these equations are vanishing (equal to zero) and the remaining six are nonvanishing. A full derivation of the Lagrange brackets can be found in Longuski's *Introduction to Orbital Perturbations* [2].

Compiling all 15 Lagrange brackets and solving for each element, we can produce the following crucial set of equations:

$$\dot{a} = \frac{2}{na}\frac{\partial \mathrm{R}}{\partial M}$$

$$\dot{e} = \left(\frac{1-e^2}{na^2e}\right)\frac{\partial \mathrm{R}}{\partial M} - \left(\frac{\sqrt{1-e^2}}{na^2e}\right)\frac{\partial \mathrm{R}}{\partial \omega}$$

$$\frac{di}{dt} = \left(\frac{cos(i)}{na^2 sin(i)\sqrt{1-e^2}}\right)\frac{\partial \mathrm{R}}{\partial \omega} - \left(\frac{1}{na^2 sin(i)\sqrt{1-e^2}}\right)\frac{\partial \mathrm{R}}{\partial \Omega}$$

$$\dot{\Omega} = \left(\frac{1}{na^2\sqrt{1-e^2}\, sin(i)}\right)\frac{\partial \mathrm{R}}{\partial i}$$

$$\dot{\omega} = \left(\frac{-cos(i)}{na^2\, sin(i)\sqrt{1-e^2}}\right)\frac{\partial \mathrm{R}}{\partial i} + \left(\frac{\sqrt{1-e^2}}{na^2e}\right)\frac{\partial \mathrm{R}}{\partial e}$$

$$\dot{M} = n - \frac{(1-e^2)}{na^2e}\frac{\partial \mathrm{R}}{\partial e} - \frac{2}{na}\frac{\partial \mathrm{R}}{\partial a}$$

Nearly identical expressions for the LPE's are provided in Vallado [3] and Battin [4].

These equations are referred to as Lagrange's Planetary Equations, and they allow us to study the gradual changes of a body's orbital elements over time when under the influence of a disturbing function. Identical

Often times it can be easier to relate the perturbative effects on the system through components of force per unit mass rather than a disturbing function. In the case of this paper's analysis, we will require further derivation of the LPE's to make this replacement.

Because of our necessity to include both conservative and non-conservative perturbative forces in our system, we will utilize the Radial-Transverse-Orthogonal force system to replace the disturbing function in the LPE's. This system is best represented using the Satellite Coordinate System – otherwise known as the RSW or Gaussian system. The force per unit mass vector is given below:

$$\vec{F} = R'\hat{u}_r + S'\hat{u}_\theta + W'\hat{u}_A$$

Force components in the RSW system for Earth's J2 effect and atmospheric drag will be derived in Part B. of this section.

To continue the derivation, we generate relations between all six partial derivatives of R and the RSW force components. These are provided below:

$$\frac{\partial R}{\partial a} = \frac{r}{a} R'$$

$$\frac{\partial R}{\partial e} = -R' \operatorname{acos} f + S' \operatorname{asin} f \left[1 + \frac{r}{a(1-e^2)}\right]$$

$$\frac{\partial R}{\partial \sigma} = \frac{R' ae \sin f}{\sqrt{1-e^2}} + \frac{S' a^2 \sqrt{1-e^2}}{r}$$

$$\frac{\partial R}{\partial \Omega} = rS' \cos i - rW' \sin i \cos i$$

$$\frac{\partial R}{\partial \omega} = S' r$$

$$\frac{\partial R}{\partial i} = \mathrm{W}' r \, sin \, u$$

The equations above can be substituted into Lagrange's Planetary Equations to generate a new set of differentials – these are referred to as Gauss's Variational Equations:

$$\dot{a} = \frac{2e \sin f}{n\sqrt{1-e^2}} R' + \frac{2a\sqrt{1-e^2}}{rn} S'$$

$$\dot{e} = \frac{\sqrt{1-e^2} \sin f}{an} R' + \frac{\sqrt{1-e^2}}{a^2 ne} \left[\frac{a^2(1-e^2) - r^2}{r}\right] S'$$

$$\frac{di}{dt} = \frac{r \cos u}{a^2 n\sqrt{1-e^2}} W'$$

$$\dot{\omega} = \frac{-\sqrt{1-e^2} \cos f}{ane} R' + \frac{\sqrt{1-e^2} \sin f}{ane} \left[1 + \frac{r}{a(1-e^2)}\right] S' - \frac{r \sin u \cot i}{a^2 n\sqrt{1-e^2}} W'$$

$$\dot{\Omega} = \frac{r \sin u}{a^2 n\sqrt{1-e^2} \sin i} W'$$

$$\dot{M} = n + \left[\frac{(1-e^2)\cos f}{ane} - \frac{2r}{a^2 n}\right] R' - \frac{(1-e^2)\sin f}{ane} \left[1 + \frac{r}{a(1-e^2)}\right] S'$$

It is important to note that we are using the following relation for mean anomaly:

$$\dot{M} = n + \dot{\sigma}$$

Again, nearly identical expressions for Gauss's form are provided in in Vallado [3].

Other variables of interest such as radius (r), true anomaly (f) and argument of latitude (u) are provided for convenience.

$$r = \frac{a(1-e^2)}{1 + e\cos f}$$

$$f = M + \left(2e - \frac{1}{4}e^3\right)\sin M + \frac{5}{4}e^2 \sin 2M + \frac{13}{12}e^3 \sin 3M + O(e^4)$$

$$u = f + \omega$$

Where the series solution of true anomaly was provided from Roy [11].

Gauss's VOP's allow us to plug in perturbative force components to generate final differential expressions which will be numerically integrated using MATLAB's ode45 function. The numerical analysis will produce the body's changing orbital elements over a selected timespan; thus, allowing for the examination of the perturbative effects on the spacecraft's trajectory.

Next, we will derive the RSW force components for J2 and Atmospheric drag.

B. Development of Perturbation Force Components

To develop perturbative force components in the Gaussian coordinate system due to Earth's oblate shape, we must first start with an expression for gravitational potential around an irregular mass:

$$U = \frac{GM}{r}\left[1 + \frac{1}{2Mr^2}(I_1 + I_2 + I_3 - 3I)\right]$$

In our analysis, we will model the earth an oblate spheroid with axial symmetry ($I_1 = I_2 = I_e$). This assumption provides a simplified relation:

$$U = \frac{GM}{r}\left[1 + \frac{1}{2Mr^2}(2I_e + I_3 - 3I)\right]$$

Using this potential function, we are able to develop an expression for the perturbative acceleration due to gravity around an oblate spheroid:

$$\vec{F} = -\left[\frac{3G(I_3 - I_e)}{2r^4}\left(1 - \frac{5z^2}{r^2}\right)\hat{u}_r + \frac{3G(I_3 - I_e)z}{r^5}\hat{u}_3\right]$$

To simplify the analysis, we can compile Earth's inertia values into a constant J. Given as:

$$J = \frac{3(I_3 - I_e)}{2M_e r_e^2} = 1.624 \times 10^{-3}$$

Now our force expression can be rewritten as:

$$\vec{F} = \frac{Jn^2a^3r_e}{r^4}\left[\left(1 - \frac{5z^2}{r^2}\right)\hat{u}_r + \frac{2z}{r}\hat{u}_3\right]$$

In the study of Earth's spherical harmonics, the perturbative force can be provided as a series solution – in which an iterating constant $J_k, k = 1,2,3, \ldots$ is used. In our simplified analysis, we will only include up to the J_2 term. The relation between our previously defined constant and J_2 is as follows:

$$J = \frac{3}{2}J_2$$

From Part A., we remember that the force components required in Gauss's Variational Equations are in the Satellite Coordinate System. Therefore, we will require a coordinate transformation to obtain the R', S', W' components.

The following relations will be used for the transformation:

$$\hat{u}_r = (c_u c_\Omega - c_i s_u s_\Omega)\hat{e}_1 + (c_u s_\Omega - c_i s_u c_\Omega)\hat{e}_2 + s_u s_i \hat{e}_3$$

$$\hat{u}_\theta = (-s_u c_\Omega - c_i c_u s_\Omega)\hat{e}_1 + (-s_u s_\Omega + c_i c_u s_\Omega)\hat{e}_2 + c_u s_i \hat{e}_3$$

$$\hat{u}_A = s_i s_\Omega \hat{e}_1 + (-s_i c_\Omega)\hat{e}_2 + c_i \hat{e}_3$$

And the above equations provide R', S', W' as follows:

$$R' = \vec{F} \cdot \hat{u}_r$$

$$S' = \vec{F} \cdot \hat{u}_\theta$$

$$W' = \vec{F} \cdot \hat{u}_A$$

Finally, we can obtain the final components of the perturbative acceleration due to Earth's J2 parameter:

$$R'_{J2} = -\frac{3}{2}\frac{J_2 \mu R^2}{r^4}[1 - 3\sin^2 i \cdot \sin^2(\omega + f)]$$

$$S'_{J2} = -\frac{3}{2}\frac{J_2 \mu R^2}{r^4}\left[\sin^2 i \cdot \sin\left(2(\omega + f)\right)\right]$$

$$W'_{J2} = -\frac{3}{2}\frac{J_2 \mu R^2}{r^4}[\sin(2i) \cdot \sin(\omega + f)]$$

The simplified form of the J2 RSW components were adapted from Curtis [5].

When these relations are plugged into Gauss's VOP's, the numerical solution will describe the motion of an orbiting body in the presence of an irregular gravitational field.

Our analysis also includes the presence of the perturbing effect of atmospheric drag. In a similar manner to the inclusion of Earth's J2 perturbation, we will derive expressions for the R', S', W' force components of the negative tangential force of drag.

An expression for drag on an orbiting body due to the trace presence of an atmosphere is as follows:

$$F = \frac{C_d A \rho V^2}{2m}$$

Because it is assumed that this force acts perfectly tangent to the orbit, it is most convenient to express drag in the Tangential-Normal-Orthogonal (NTW) force system. Given as follows:

$$\vec{F} = T'\hat{u}_T + N'\hat{u}_N + W'\hat{u}_A$$

Therefore, we obtain:

$$T' = -\frac{C_d A \rho V^2}{2m},\ N' = 0,\ W' = 0$$

But due to the fact that the expressions provided for Gauss's Variational Equations in Part A. use R', S', W' force components, it will be most convenient to convert from the NTW system to the RSW system. This conversion occurs through the following relations:

$$R' = \frac{T' e \sin f}{(1 + e^2 + 2e\cos f)^{1/2}} - \frac{N'(1 + e\cos f)}{(1 + e^2 + 2e\cos f)^{1/2}}$$

$$S' = \frac{T'(1 + e\cos f)}{(1 + e^2 + 2e\cos f)^{1/2}} + \frac{N' e \sin f}{(1 + e^2 + 2e\cos f)^{1/2}}$$

Inserting drag's T', N' components above , we finally arrive at the R', S', W' values used to describe the perturbative acceleration on an orbiting body from atmospheric drag:

$$R'_{Drag} = \frac{e \sin f}{(1 + e^2 + 2e\cos f)^{\frac{1}{2}}}(-b\rho V^2)$$

$$S'_{Drag} = \frac{1 + e\cos f}{(1 + e^2 + 2e\cos f)^{\frac{1}{2}}}(-b\rho V^2)$$

$$W'_{Drag} = 0$$

Where the ballistic coefficient (b) is given as,

$$b = \frac{C_D A}{2m}$$

And velocity (V) is given as,

$$V^2 = \frac{h^2}{a^2(1 - e^2)^2}(1 + 2e\cos f + e^2)$$

Lastly, it is important to note that we will use a simplified Earth standard atmosphere in MATLAB to obtain values of density (ρ) at the corresponding altitudes. The model was adapted from Curtis [5].

Now we have derived perturbative force components in the Satellite Coordinate Frame for both drag and the J2 parameter. To include both effects in our numerical integration of Gauss's Variational Equations, we must sum the components. The final values will become:

$$R' = -\frac{3}{2}\frac{J_2 \mu R^2}{r^4}[1 - 3\sin^2 i \cdot \sin^2(\omega + f)] + \frac{e \sin f}{(1 + e^2 + 2e\cos f)^{\frac{1}{2}}}(-b\rho V^2)$$

$$S' = -\frac{3}{2}\frac{J_2 \mu R^2}{r^4}\left[\sin^2 i \cdot \sin\big(2(\omega + f)\big)\right] + \frac{1 + e\cos f}{(1 + e^2 + 2e\cos f)^{\frac{1}{2}}}(-b\rho V^2)$$

$$W' = -\frac{3}{2}\frac{J_2 \mu R^2}{r^4}[\sin(2i) \cdot \sin(\omega + f)]$$

Now we have all that is required to develop a numerical propagation of an artificial satellite under the effects of drag and Earth's oblate shape.

C. Critical and Heliosynchronous Inclinations

In the next portion of this report, the previously derived dynamic model is used to analyze several orbits of interest – primarily sun synchronous and critically inclined orbits under 600 km. Unlike most other orbits, these are of special interest to our study due to their initial conditions. Both orbits utilize the unique nature of the perturbative effects of Earth's oblate shape to optimize aspects of their mission.

In order to better understand this methodology and derive the correct initial conditions, we must examine differential rates of the *mean* orbital elements – specifically argument of periapsis (ω) and right ascension of ascending node (Ω).

The most practical method of developing differential relations for the mean orbital elements will be to use Lagrange's Planetary Equations which have been provided in Part A. As a reminder, the LPE's require a disturbing function to model the perturbative force on the orbiting body. From the gravitational potential provided previously and further derivation in Battin, we can generate the following [4]:

$$R = -\frac{GmJ_2 r_e^2}{2p^3}[1 + e\cos f]^3[3\sin^2 u \sin^2 i - 1]$$

To study the motion of the mean orbital elements, we must find an averaged solution of the R over one orbit – denoted as $\overline{R}$.

$$\overline{R} = \frac{1}{2\pi}\int_0^{2\pi} \frac{n}{h} R r^2 df$$

The integration will provide,

$$\overline{R} = \frac{n^2 J_2 r_e^2}{4(1-e^2)^{\frac{3}{2}}}(2 - 3\sin^2 i)$$

We immediately notice that $\overline{R}$ is not a function of Ω, ω, or M, therefore the following LPE differentials vanish:

$$\overline{\frac{da}{dt}} = 0, \overline{\frac{de}{dt}} = 0, \overline{\frac{di}{dt}} = 0$$

And by obtaining the required partial derivatives of $\overline{R}$, we find the following:

$$\overline{\frac{d\omega}{dt}} = \frac{3}{4} J_2 \left(\frac{r_{eq}}{p}\right)^2 n(5\cos^2 i - 1)$$

$$\overline{\frac{d\Omega}{dt}} = -\frac{3}{2} J_2 \left(\frac{r_{eq}}{p}\right)^2 n \cos i$$

Where the variables of interest are given as,

$$n = \sqrt{\frac{\mu}{a^3}}$$

$$p = a(1 - e^2)$$

These expressions are identical to those derived in Battin [4].

The vanishing equations for a and e will be ignored in this analysis, but it will be important to note that the expression $\overline{\frac{di}{dt}} = 0$ proves that under a J2 perturbation, the mean inclination will remain constant. Relations describing the rates of ω and Ω both depend on this constant orbital inclination; therefore, allowing for special i_0 values to uniquely manipulate the outcome of the rates.

From the $\overline{\frac{d\omega}{dt}}$ expression, it is apparent that there exists an inclination that will remove any regression in the argument of periapsis – this value is often referred to as the *critical inclination.*

$$0 = \frac{3}{4} J_2 \left(\frac{r_{eq}}{p}\right)^2 n(5\cos^2 i - 1)$$

Solving the equation above will yield the required inclination to stop the orbiting body from experiencing any change in mean argument of periapsis. Battin provides this value as:

$$i_{crit} = 63°26'.1 \text{ [4]}$$

In a similar vein, we can analyze the $\overline{\frac{d\Omega}{dt}}$ expression to determine an initial inclination for a sun-synchronous orbit. In this orbit regime, the spacecraft's nodal regression due to Earth's J2 parameters is used to perfectly match the rate of Earth's rotation around the sun [6]. Therefore, the following expression is used:

$$\overline{\frac{d\Omega}{dt}}_{J2} = \frac{d\Omega}{dt}_{Sun} \approx 0.19910213 * 10^{-6} \text{ rad/s } \text{ [7]}$$

Contrasting the critical inclination, the required SSO inclination depends on the semi-major axis of the orbit – thus, i_0 varies based on the initial radius of the orbit. The following relation allows for the determination of the correct sun synchronous inclination for a specific orbit.

$$i_{SSO} = \cos^{-1}\left[-\frac{2}{3}\frac{d\Omega}{dt}_{Sun}\frac{1}{J_2}\left(\frac{a_0(1-e_0^2)}{Re}\right)^2\sqrt{\frac{a_0}{\mu}}\right] \text{ [7]}$$

With the expressions for both critical and sun synchronous inclinations, we are now able to propagate and analyze artificial satellites in these orbits.

III. Numerical Results and Discussion

A dynamic model including perturbative effects of Earth's oblate shape and atmospheric drag has been derived and will be numerically solved using MATLAB. The following section will define an initial test orbit to examine the effects of the J2 and drag perturbations individually and when combined. Then, sun synchronous and critically inclined near-earth orbits will be defined, and their resulting trajectories and orbital decay will be studied. Additionally, weaknesses in the dynamic model are also discussed.

A. Development of the Numerical Model

To study the perturbative effects of drag and the J2 parameter, we begin with propagation of a test orbit defined below:

Table 1. Initial Conditions for Dynamic Model Test Orbit [5]

	Apogee (km)	Perigee (km)	Inclination (degrees)	Longitude of Ascending Node (degrees)	Argument of Perigee (degrees)	True Anomaly (degrees)
Initial Conditions	160	939	28.45	339.94	58	332

Due to the separate derivation of the perturbative acceleration components in Section 1, the model is able to toggle between J2 only, drag only, or both J2 and drag. We will begin my analyzing the effects of both perturbations separately, then perform the same study when they are combined. For the test case, the orbit was propagated for 15 days.

1. J2 Only Case

In the J2 only case, we happened to derive differential equations for both the averaged and non-averaged cases in Section 1. The averaged case is simple enough to solve analytically, while the non-averaged solution must be performed numerically. As validation of our model, the test orbit was propagated using both solutions for this specific case.

Over the 15-day timespan, the model produced the following results for the satellite's orbital elements:

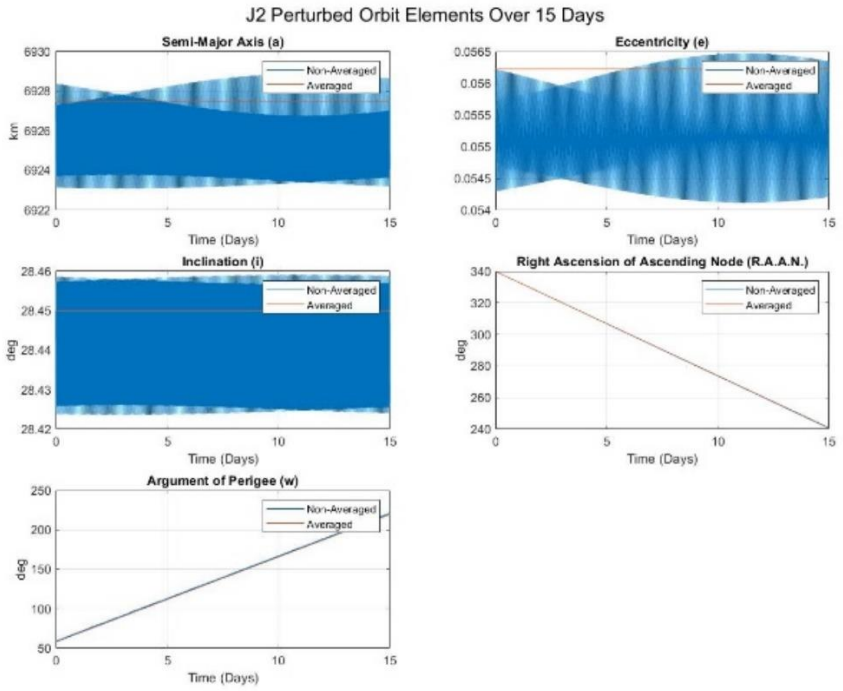

Figure 1. Averaged and Non-Averaged J2 Perturbed Test Orbit

From Figure 1, it becomes clear that perturbations due to Earth's oblate shape (up to the J2 parameter), primarily disturb the argument of perigee and longitude of ascending node. The other elements remain constant (averaged case) or nearly constant (non-averaged case) through the propagation.

Additionally, Figure 1 helps validate our numerical solution, as it significantly matches the analytical mean solution. While it contains heavy oscillations for all elements, the secular nature of RAAN and argument of perigee remains, while the remaining elements display short amplitude oscillations which become negligible in our LEO case.

A visual of the orbit around earth is provided below:

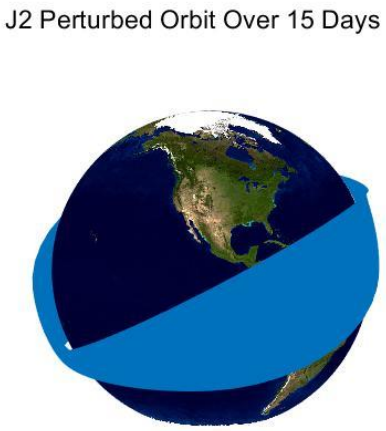

Figure 2. J2 Perturbed Test Orbit Around Earth

From Figure 2, we clearly observe the secular behavior of the argument of perigee and RAAN, as both elements regress over the 15-day timespan.

2. Drag Only Case

Next, we can examine the same test orbit under only the effects of atmospheric drag. To calculate the ballistic coefficient of our orbiting satellite, we can use the following data for a hypothetical spherical object.

Table 2. Ballistic Coefficient Data for Spherical Test Satellite [5]

	Cd	Mass (kg)	Cross Sectional Radius (m)
Satellite Data	2.2	300	3

The results of the numerically integrated orbital elements over a 15-day timespan are displayed below:

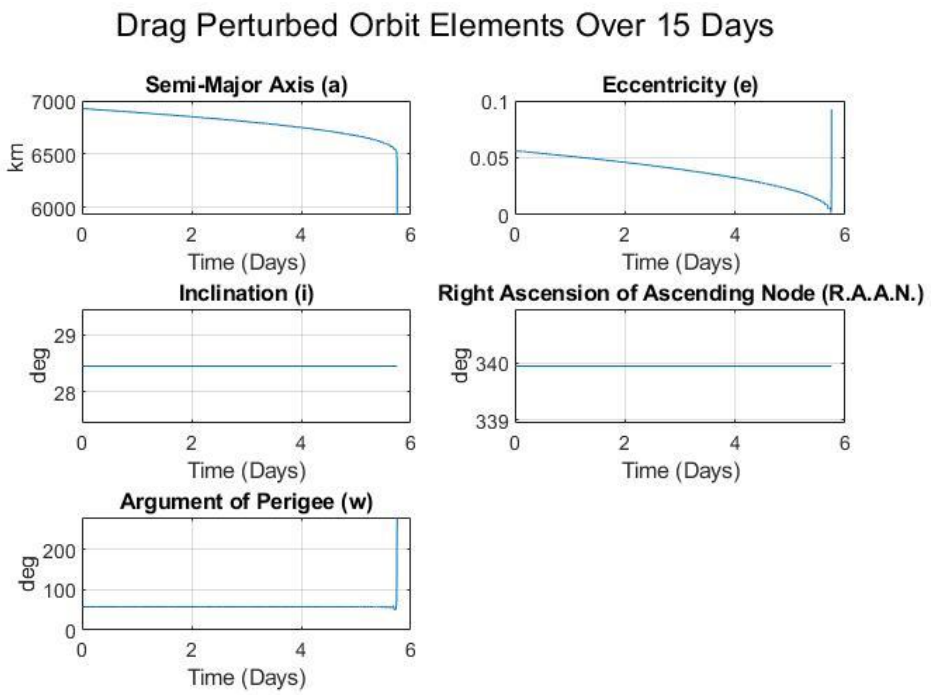

Figure 3. Orbital Elements of Drag Perturbed Test Orbit

Figure 3. does a great job of clearly displaying the orbital elements effected by atmospheric drag – only semi major axis and eccentricity are affected in this case. These results are logical due to the fact that the perturbative acceleration component of W' is equal to zero; therefore, inclination, RAAN and argument of perigee will be undisturbed.

It is also noticeable that the simulation did not last the full 15-day lifespan – ending after only 5.75 days. The model has been programmed to end the propagation once the perigee of the orbit drops below 90km. At this altitude, the orbit has re-entered the atmosphere and can no longer be propagated. We can record this time, thus yielding a numerically generated lifetime of the satellite.

The reduction of the orbit's semi-major axis and eccentricity can be noted in plot of the elements, but the following figure displays the decay of the orbital altitude over time:

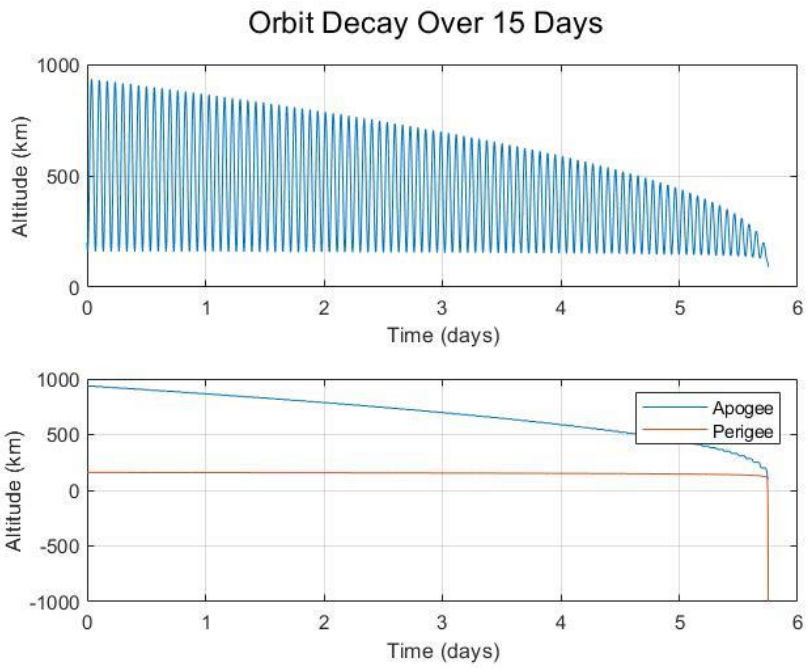

Figure 4. Drag Induced Orbit Decay of Test Orbit

Figure 4. displays the graduate decline in the test orbit until atmospheric re-entry. One clear discovery is that the apogee distance is the primary value that decays over the timespan, while the perigee remains nearly constant until full decay.

The drag only case can be visualized around earth below:

Figure 5. Drag Perturbed Test Orbit Around Earth

The 3-dimensional earth orbiting display in Figure 5. allows for a visualization of the decrease in semi major axis and eccentricity through the orbit lifetime. Additionally, the findings from Figure 4 can be seen as the apogee side of the orbit experiences a significant decline, while the perigee side remains nearly constant.

3. Combined Drag and J2 Case

Now that drag and J2 perturbations have been studied individually, the dynamic model is able to combine both to develop a new case. The test orbit conditions and satellite data in Tables 1 and 2 are still used. The results of the orbital elements is seen below:

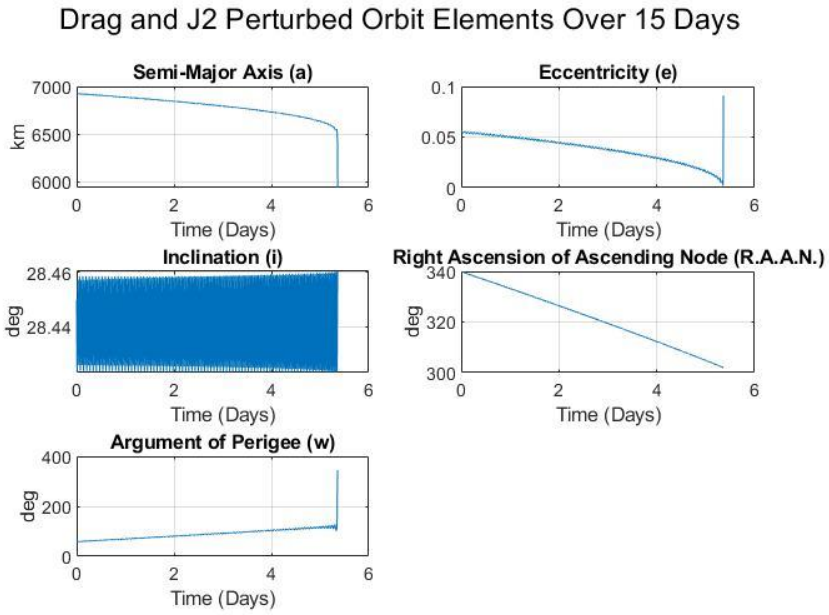

Figure 6. Orbital Elements of Combined Drag and J2 Perturbed Test Orbit

In the drag only case the elements of interest were semi-major axis and eccentricity, while in the J2 only case the elements of interest were the RAAN and argument of perigee. When combining both perturbations, Figure 6 shows that these four elements have continued the trends seen in their individual cases, leaving just inclination to remain nearly constant (with minor oscillations). This helps to prove that the perturbative accelerations for atmospheric drag and earth's J2 parameter remain largely independent.

Similar to the drag only case, the test orbit eventually re-enters the atmosphere. The altitude decay can be seen below:

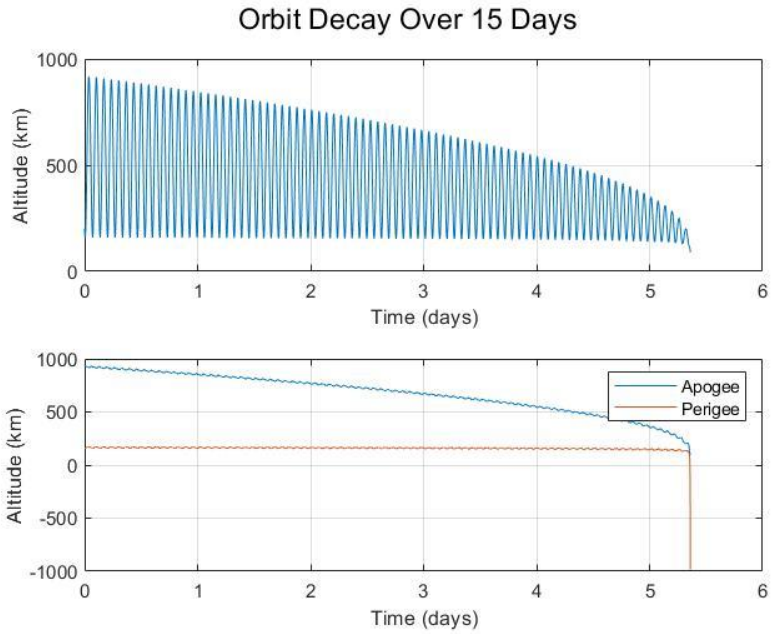

Figure 7. Orbit Decay of Drag and J2 Perturbed Test Orbit

The plot of orbit decay for the combined case has deviated very little from the drag only case shown in Figure 5. Again, this does make sense as the J2 perturbation imposes nearly no effect to semi-major axis and eccentricity. Interestingly, the lifespan of the satellite in the combined case is 5.36 days – which is slightly smaller than the lifespan of the drag only case. Therefore, we see that the J2 generated short period oscillations of semi-major axis and eccentricity do slightly affect the decay of the system.

Again, we plot the propagated orbit around the earth.

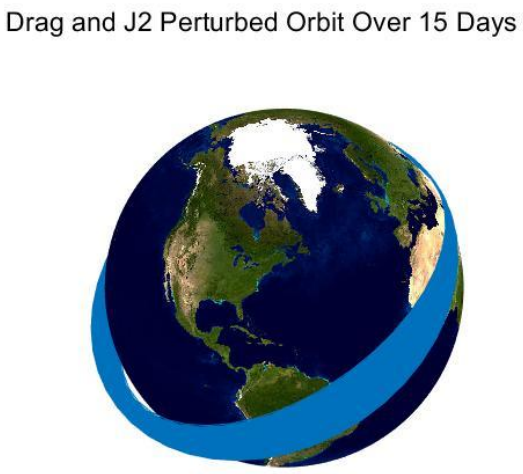

Figure 8. J2 and Drag Perturbed Test Orbit Around Earth

The conclusions generated from the behavior of the orbital elements are better visualized in the 3d display in Figure 8.

The dynamic model has been fully developed and analyzed, and it is now ready to be used to examine behavior of specific orbits.

B. Sun Synchronous Orbits

The first orbit that will be examined with our J2/Drag numerical propagator will be the Sun Synchronous Orbit. As derived and explained in Section 1, the initial inclination of the orbit is chosen based on the initial orbit radius. The following plot shows a general trend of this relationship:

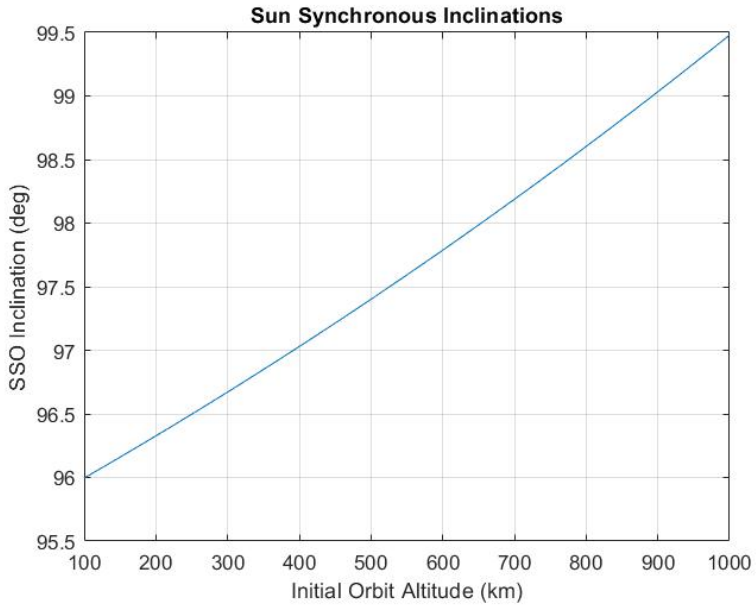

Figure 9. Initial Inclination for Initial Orbit Radius

Most sun synchronous orbits are very close to circular, but Gauss's Variational Parameters experience a singularity when eccentricity falls to zero; therefore, we will separate our apogee and perigee radii by at least 50 km.

1. 600 km Sun Synchronous Orbit

The analysis will begin with a ~600 km orbit with initial conditions given below:

Table 3. Initial Conditions for 600 km Sun Synchronous Orbit [7]

	Apogee (km)	Perigee (km)	Inclination (degrees)	Longitude of Ascending Node (degrees)	Argument of Perigee (degrees)	True Anomaly (degrees)
Initial Conditions	650	550	97.7865	100	0	0

To heighten accuracy of the simulation, we will use public data from the Resurs-DK1 satellite – which was launched into similar LEO conditions.

Table 4. Ballistic Coefficient Data for Resurs-DK1 Satellite [8]

	Cd	Mass (kg)	Cross Sectional Area (m^2)
Satellite Data	3.3	6804	15

With these parameters, we can propagate our satellite over a fifty-day timespan. The resulting behavior of the orbital elements are shown below:

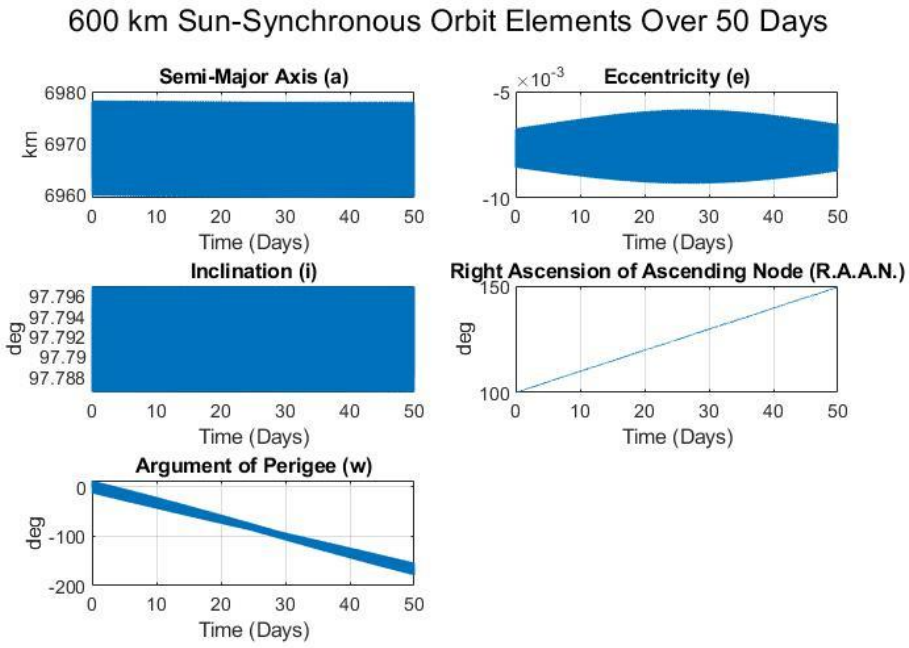

Figure 10. Orbital Elements of 600 km Sun Synchronous Orbit

From Figure 10, we see that the effects of drag on the semi-major axis and eccentricity are very minimal; therefore, it becomes clear that drag at this altitude provides little perturbative effects. The secular nature of RAAN and argument of perigee are still present and nearly linear. Argument of perigee does experience a larger than usual short period oscillation, but RAAN –used to match Earth's nodal regression around the sun – remains stable. Most importantly, the inclination, which keeps the RAAN regressing at the correct rate, remains very stable through the propagation; while short period oscillation occurs, we can conclude that a sun-synchronous orbit at this altitude would remain in the correct orientation relative to the sun for an extended period of time.

To study drag's effects on this orbit in more detail, a plot of the orbit decay is produced:

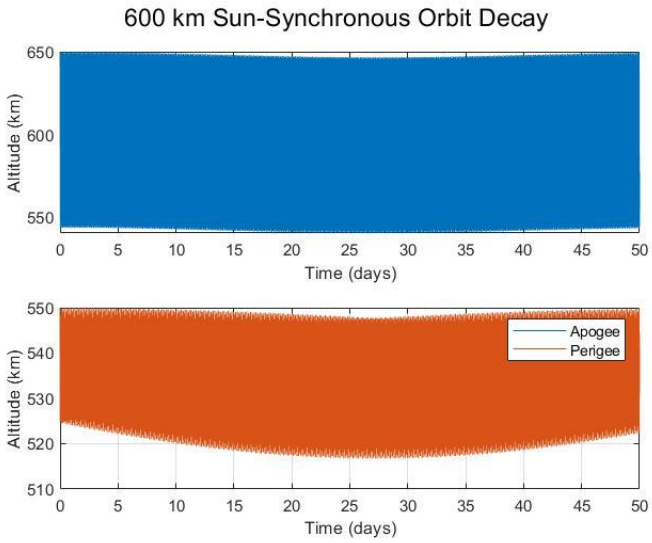

Figure 11. Orbital Decay of 600 km Sun Synchronous Orbit

Figure 11 reinforces the lack of semi-major axis and eccentricity change observed in Figure 10. The orbit experiences very little decay over the 50-day timespan, so a satellite in this configuration would require far less station keeping. A three-dimensional plot of the trajectory is also seen below:

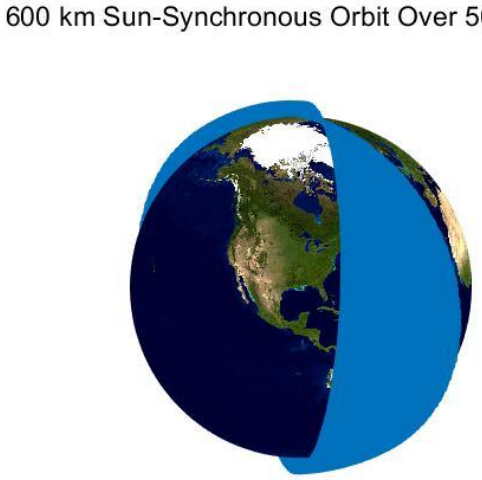

Figure 12. 600 km Sun Synchronous Orbit Around Earth

Again, we see the clear regression of both the RAAN and argument of perigee with very little drop in periapsis. Figure 12 helps display how this nearly polar inclination keeps the satellite at the same orientation to the sun through its lifespan.

2. 275 km Sun Synchronous Orbit

The propagation of the 600 km sun synchronous satellite displayed the fundamental properties of its orbit with minimal drag induced decay. Now we can analyze a similar scenario closer to Earth – at 275 kilometers.

The satellite data will remain the same as what was given in Table 4, but new initial conditions are given below:

Table 5. Initial Conditions for 275 km Sun Synchronous Orbit [7]

	Apogee (km)	Perigee (km)	Inclination (degrees)	Longitude of Ascending Node (degrees)	Argument of Perigee (degrees)	True Anomaly (degrees)
Initial Conditions	250	300	96.5841	100	0	0

It is important to note that our new radius provides us with a new SSO initial inclination from the derived formula in Section 1c. The orbital elements for a 50-day propagation are provided:

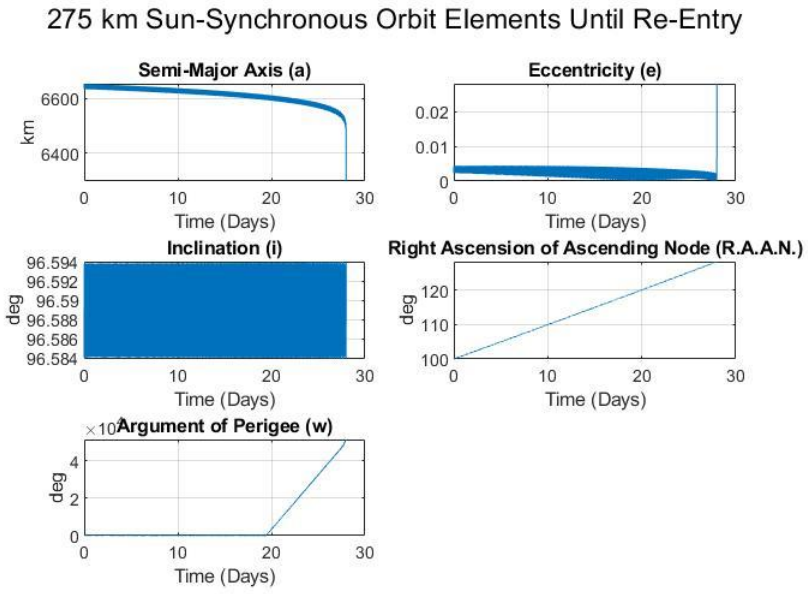

Figure 13. Orbital Elements of 275 km Sun Synchronous Orbit

Unlike before, the lower 275 km orbit experiences a far more significant decay in semi major axis and eccentricity which leads to atmospheric re-entry at 27.9 days. Similar to the first case, the inclination remains nearly constant with a minor small period oscillation (negligible), and the RAAN exhibits almost linear secular behavior. An important observation from Figure 13 is that the plot for argument of perigee looks vastly different than expected, as the angle explodes around 20 days into the propagation. This occurs due to the fact that eccentricity exists in the denominator of the $\dot{\omega}$ differential. When the eccentricity drops to a low enough value, the rate of change for argument of perigee expands extremely rapidly – until a singularity at e = 0. This is a severe weakness of the dynamic model, and the inclusion of drag exacerbates the issue.

The decay of the 275 km sun synchronous orbit can also be visualized below:

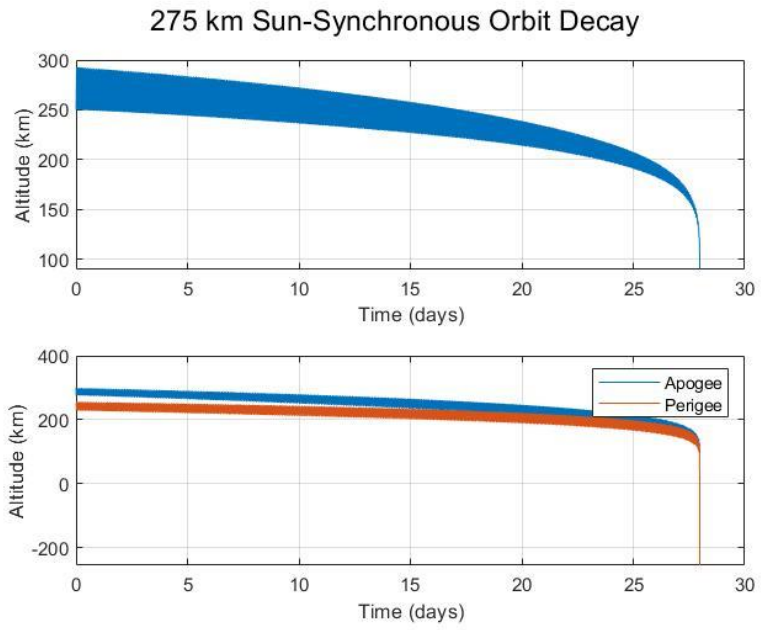

Figure 14. Orbital Decay of 275 km Sun Synchronous Orbit

Due to the nearly circular nature of a SSO, both the apogee and perigee decline at similar rates. Once the satellite approaches 150 km, it experiences significant decay from the exponentially thicker atmosphere; finally re-entering after 28 days in orbit.

The satellites trajectory can also be visualized around the earth:

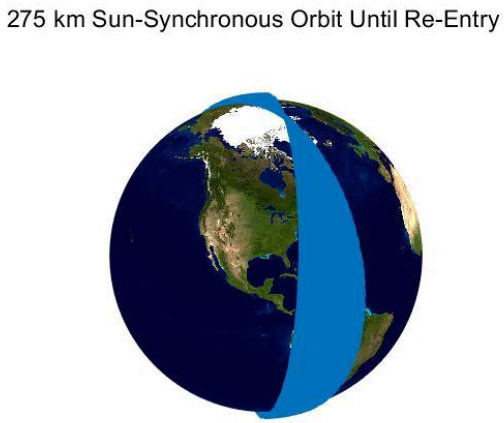

Figure 15. 275 km Sun Synchronous Orbit Around Earth

Due to the shorter lifespan and lower orbit, the satellite experiences less nodal regression than the 600 km orbit.

3. Numerical Lifetime Analysis of a Sun Synchronous Orbit

Reducing the orbit radius from 600 to 275 kilometers reduced the lifetime of the orbit significantly. This is due to the exponential behavior of earth's atmospheric density. To obtain a clearer picture of approximate sun synchronous orbit lifetimes, we can run the numerical simulation at multiple different altitudes until re-entry. The results are visualized below:

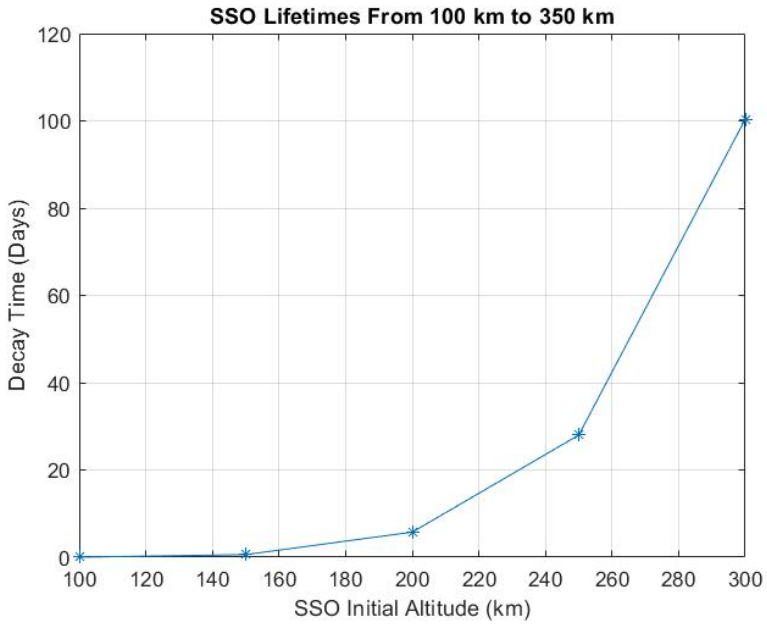

Figure 16. Lifetime of Sun Synchronous Orbits from 100 to 350 km

The results of this numerical lifetime analysis provide an exponential rise in re-entry time as initial orbit radius increases. The short lifespans of orbits under 300 km make them impractical for long term missions, as the station keeping requirements would be far too great. Therefore, circular orbits (such as sun synchronous satellites) should be established above this threshold. Orbits beyond 300 km did not decay within a simulation of 300 days, and it is too computationally intensive to continue. Further analysis can be done using averaged analytical solutions with only drag.

C. Critically Inclined Orbits

Similar to sun synchronous orbits, low earth critically inclined orbits also require the presence of perturbations due to Earth's J2 parameter, and are adversely affected by the atmosphere; therefore, these orbits are great candidates for examination by our drag/J2 dynamic model.

We will use the same satellite data from the Resurs-DK1 Satellite in Table 3. The initial orbital conditions are as follows:

Table 6. Initial Conditions for 275 km Critically Inclined Orbit [7][9]

	Apogee (km)	Perigee (km)	Inclination (degrees)	Longitude of Ascending Node (degrees)	Argument of Perigee (degrees)	True Anomaly (degrees)
Initial Conditions	250	300	63.4	100	270	0

With these parameters, we can propagate our satellite over a fifty-day timespan. The resulting behavior of the orbital elements are shown below:

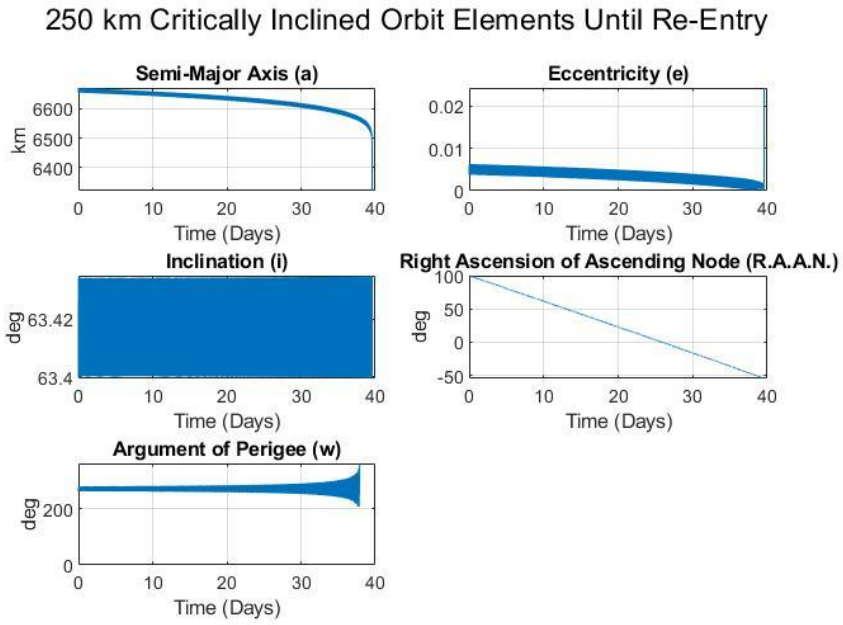

Figure 17. Orbital Elements of 275 km Critically Inclined Orbit

The majority of the orbital elements continue to exhibit the same behaviors as the test and sun synchronous orbits, but Figure 17 shows a uniquely constant argument of perigee through the orbit timespan. As derived in section 1, the critical inclination creates a constant mean rate of argument of perigee – thus, stopping the normally secular regression of this element. While it still contains a short period oscillation that grows during atmospheric re-entry, the variance is nearly negligible to the orbit. It is a vital discovery to see that the theoretical derivation of this initial inclination performs nominally in the numerical integration. It is also important to note that the inclination varies very little from the initial value provided, which allows for this behavior to occur.

The numerical results in Figure 17 show us that a critically inclined orbit can be incredibly advantageous for satellites that require limited orbital regression in order to maintain ground tracks in the same regions. Due to the perturbative effects of Earth's oblate shape, manual corrections to the orbit will normally be required to control the secular RAAN and argument of perigee values over long timespans. In this unique case, the regression of ω can be significantly minimized – thus reducing station keeping requirements of the mission. This is one example of a "frozen orbit", and

it has been used extensively in many cases. For example, the soviet Molniya orbit is a critically inclined, highly eccentric orbit that allowed for the constant satellite ground track of the northern hemisphere (impossible even in GEO)[9].

As before, we can also analyze the orbit decay below:

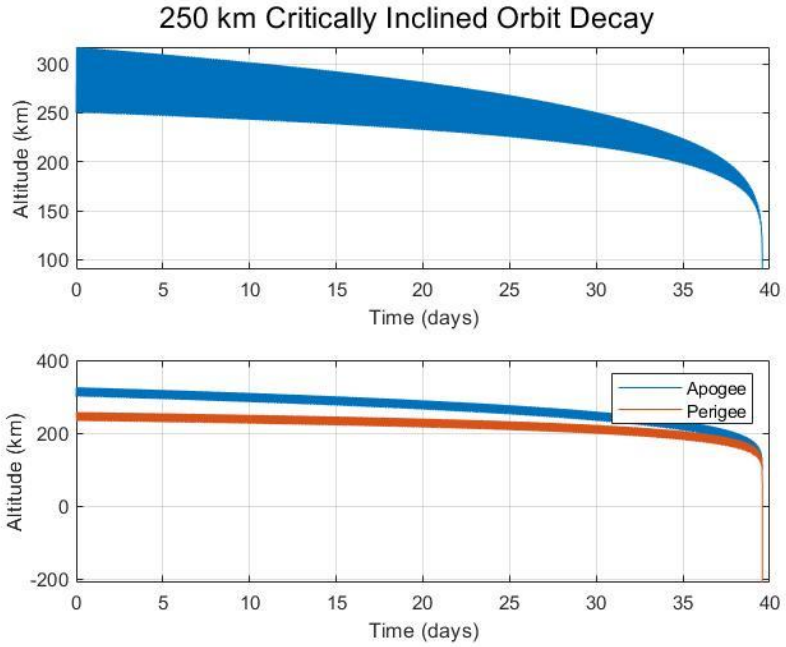

Figure 18. Orbital Decay of 275 km Critically Inclined Orbit

The decay for the critically inclined orbit looks extremely close to the sun synchronous orbit. This does make sense as both are nearly circular with the same starting radii. But this orbit has a longer lifespan of 39.5 days, which is not clearly explained. This longer time to re-entry may be a product of the short period oscillations that the J2 perturbation induces on semi-major axis and eccentricity.

Further decay analysis can be performed in a similar manner to the sun synchronous orbits. The orbit lifetimes from 100 to 350 km are shown below:

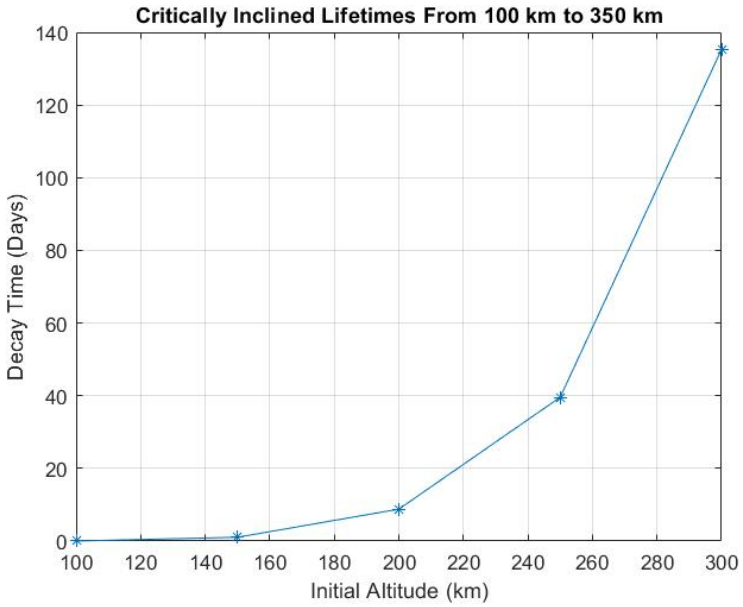

Figure 19. Lifetime of Critically Inclined Orbits from 100 to 350 km

Again, we notice a steep exponential increase in lifetimes as the initial radii rise. Since both critical and sun synchronous orbits are circular, their lifetime analysis should be nearly identical. From Figure 19, it becomes clear that any critically inclined orbit satellite should be placed above 300 km to reduce significant amounts of orbit raising maneuvers.

D. Weaknesses in Highly Elliptical Orbits

While performing analysis with the dynamic model derived in this report, a significant weakness was discovered in relation to highly eccentric orbits. As discussed previously, Soviet Molniya orbits are prominent examples of mission design based upon the principle of critical inclination. When attempting to propagate these orbits, strange behavior in the orbital elements was noticed.

When drag was removed from the model (J2 became the sole perturbation), the satellite was re entering the atmosphere. This is problematic due to the fact that Earth's oblate shape should not be supplying perturbative accelerations which decay the orbit. A similar study was done using the highly elliptic geostationary transfer orbit. Initial conditions are given in the table below:

Table 7. Initial Conditions for GTO Satellite [10]

	Apogee (km)	Perigee (km)	Inclination (degrees)	Longitude of Ascending Node (degrees)	Argument of Perigee (degrees)	True Anomaly (degrees)
Initial Conditions	35786	200	28.5	190	180	180

From these initial conditions, we can produce the following results for orbital elements and decay:

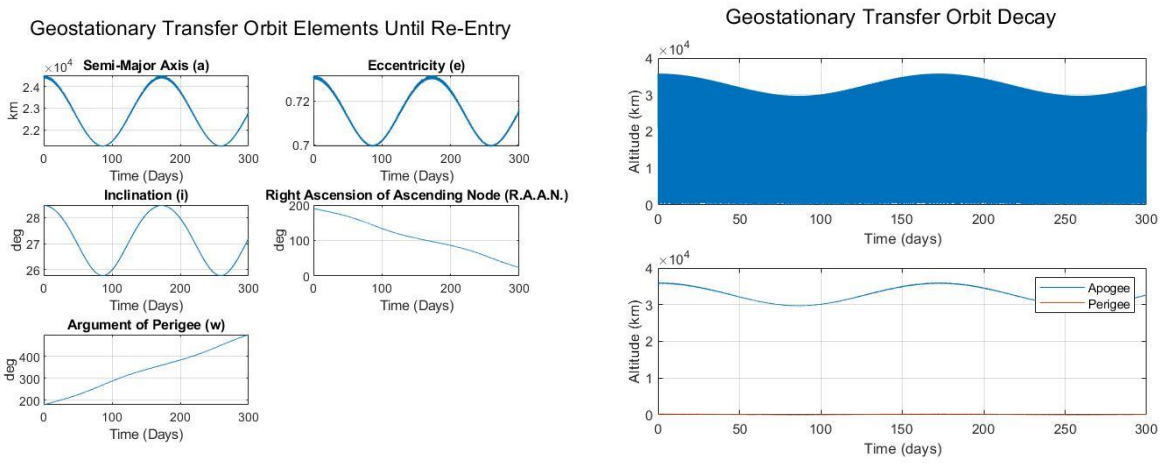

Figure 20. Orbital Elements and Decay of GTO Satellite

We notice that the semi-major axis, eccentricity, and inclination experience long and short period oscillations through the 300-day timespan. Most critically, the semi-major axis contracts by nearly 200 kilometers at its lowest point. While this is a small amplitude relative to the total semi-major axis of the geostationary transfer orbit (due to the high apogee), it can cause significant lowering of the periapsis. Initially at 200 km, the perigee is already dangerously close to re-entry, and due to these oscillations, it drops to 5 km at its lowest point in the simulation. Therefore, J2 alone caused full orbit decay of a GTO spacecraft – this is not realistic.

This an important limitation of the dynamic model derived in this report, and further analysis must be done to remove this weakness.

IV. Conclusions and Future Work

1. Earth's J2 parameter induces secular behavior of RAAN and Argument of Periapsis, while drag contracts semi-major axis and eccentricity.

When numerically solving the dynamic model derived in this report, different trends were noticed for each orbital element. Differential equations for the mean orbital elements showed that Earth's J2 parameter induced secular behaviors for the RAAN and argument of periapsis while all other elements remained constant. Additionally, the perturbative acceleration components for drag hypothetically should never affect elements other than semi-major axis, eccentricity, and argument of periapsis. When combining these perturbations, we see that the hypothesized behaviors from the equations behind the model were very accurate with some exceptions.

The J2 parameter generated clearly secular trends for both RAAN and argument of periapsis (unless at critical inclination), and three-dimensional plots of the propagated orbit trajectory displayed the regression of the orbit for every case analyzed. Because the model used non-averaged elements, semi-major axis, eccentricity, and inclination did not remain constant – instead they experienced short period oscillations that, for the most part, were negligible to the overall system. These oscillations did not significantly affect the trajectory of the artificial satellite unless under unique highly eccentric circumstances (discussed in part 4.).

Atmospheric drag primarily contracts the semi-major axis and eccentricity of an orbit, but it also should affect the argument of periapsis. In the numerical results, the decay of the semi-major axis and eccentricity was primarily clear – especially in lower, more drag affected orbits. The contraction of these two elements also produced full atmospheric re-entry for several cases analyzed in the paper; therefore, allowing for the calculation of approximate satellite lifetimes. Drag influenced argument of periapsis in a far lower capacity, but it was seen to induce an oscillatory behavior in conjunction with the J2 perturbation. All other orbital elements were unaffected by drag.

2. Perturbations from atmospheric drag and Earth's oblate shape minimally effect the orbital inclination.

The most unaffected orbital element in all scenarios examined in this report was the inclination. While the J2 parameter produced slight oscillatory behavior to the element, the amplitude always remained small enough to keep the variance negligible. Additionally, the period and amplitude of the oscillations remained nearly constant throughout long timespan propagation – again proving its minimal response to the J2 perturbation. Drag also did not seem to take any effect in all cases that were studied.

This fact is quite important due to the fact that both sun synchronous and critically inclined orbits required a specific inclination to be held throughout the time period of the propagation in order to meet mission objectives. For the SSO case, drift in inclination would cause the RAAN to no longer match the nodal precession of the earth in relation to the sun; thus, ceasing the primary benefit of the orbit. In the critically inclined case, a drift in inclination would revert the argument of periapsis to its secular behavior – causing unwanted excess precession in the orbit. This fact was exceptionally clear in Figure 17 as the argument of periapsis remained nearly constant (with negligible oscillations) for the entire lifetime of the satellite. If inclination began to drift, this would not have been the case.

Overall, this fact is very important for mission design, as we can be more sure that the two most influential LEO perturbations do little to effect inclination; therefore, allowing for less station-keeping requirements of orbits that necessitate constant inclinations.

3. The lifetime of near-circular low earth orbits increases exponentially as initial altitude is raised.

Lifetimes for the near circular sun synchronous and critically inclined orbits were generated at different altitudes in Figures 16 and 19. From this data, we are able to determine that the time until re-entry exponentially rises as the initial radius is raised through the low earth orbit regime. This is mathematically supported by the fact that the atmosphere experiences a near exponential decrease from the 100 to 500 km altitudes. Therefore, these results show that small increases in initial orbit altitude can produce large gains in overall satellite lifespans. Just increasing an orbit from 200km to 300 km will allow a satellite to live nearly 100 more days; a giant gain for relatively low propulsive cost. Another important fact in space mission design.

A future addition to this analysis would be the inclusion of an analytic solution to lifespan of a drag perturbed orbit. Calculating the time of orbit re-entry using numerical integration techniques is computationally expensive; thus, greatly limited the lifetime analysis performed in this report. An analytical solution exists, so its admittance would be a logical next step.

4. Long period oscillations from Earth's J2 parameter cause unrealistic decay in highly eccentric orbits.

While performing analysis with the dynamic model derived in this report, a significant weakness was discovered in relation to highly eccentric orbits. The numerical integration of this model has produced long and short period perturbations for the semi-major axis and eccentricity for all cases that were studied. The amplitude of these oscillations has often been quite small in relation to the initial value of the elements – therefore, allowing the variation to remain negligible through the propagation. But when using initial conditions of a highly elliptical orbit with a low perigee and high apogee, the relatively small amplitude of semi-major oscillations is large enough to cause premature decay of the orbit. Even when drag is removed as a perturbation, these J2 induced oscillations can cause perigee to drop under 100 km; thus, killing the orbit. Figure 20 displays this problematic behavior in a GTO example – where the orbit contracted to 5 km in only ~50 days. This effect is highly unrealistic and is a major drawback to the dynamic model. It will be important to keep in mind that it is not recommended to examine highly eccentric orbits, such as Molniya or GTO, with this model. Further analysis and study must be done to determine the root cause and how to correct the issue.

V. References.

[1] Longuski, J.M. *AAE 690: Orbital Perturbations*, Purdue University, West Lafayette, IN. 2022.

[2] Longuski, J.M., Pollock, G.E., and Hoots, F. *Introduction to Orbital Perturbations*, Springer International Publishing, Space Technology Library, 2022.

[3] Vallado, David A., and Wayne D. McClain. *Fundamentals of Astrodynamics and Applications*. Microcosm Press, 2013

[4] Battin, R.H., *An Introduction to the Mathematics and Methods of Astrodynamics.* AIAA Education Series. New York, 1987.

[5] Curtis, H.D., *Orbital Mechanics for Engineering Students.* Elsevier Aerospace Engineering Series. Cambridge, MA, 2020.

[6] Boain, R.J., *A-B-Cs of Sun-Synchronous Orbit Mission Design*, 14th AAS/AIAA Space Flight Mechanics Conference, Maui, Hawaii, 2004.

[7] *J2 Perturbation*, FreeFlyer University Guide. A.I Solutions. https://aisolutions.com/_freeflyeruniversityguide/j2_perturbation.htm.

[8] Zhejun, et al., *Estimation of ballistic coefficients of space debris using the ratios between different objects*, Chinese Journal of Aeronautics, Volume 30, Issue 3, 2017.

[9] Hoogland, J., *Earth Frozen Orbits: Design, Injection and Stability*, Masters of Science Thesis, TU Delf, 2015.

[10] Janin, G., *Lifetime of Objects in Geostationary Transfer Orbit*, Workshop on Salyut 7 / Kosmos-1686 Reentry, Darmstadt, 1991.

[11] Roy, A.E., *Orbital Motion.* Adam Hilger, Bristol and Philadelphia. 1988.

VI. Appendix

All MATLAB code is published and attached on the next page.